ACS APPLIED MATERIALS & INTERFACES

Research Article

www.acsami.org

Tuning Electrical Properties in Amorphous Zinc Tin Oxide Thin Films for Solution Processed Electronics

R. Devi Chandra,[†,#] Manohar Rao,[†,#] Keke Zhang,[†] Rajiv Ramanujam Prabhakar,[†] Chen Shi,[‡] Jie Zhang,[⊥] Subodh G. Mhaisalkar,[†,§,⊥] and Nripan Mathews*[,†,§,¶]

[†]Energy Research Institute, Nanyang Technological University, Singapore 637553

[‡]School of Physical and Mathematical Sciences, Nanyang Technological University, Singapore 637371

[§]School of Materials Science and Engineering, Nanyang Technological University, Singapore 637553

[⊥]Institute of Materials Research and Engineering, 3 Research Link, Singapore 117602

[¶]Singapore-Berkeley Research Initiative for Sustainable Energy (SinBeRISE), 1 Create Way, Singapore 138602

Supporting Information

ABSTRACT: Solution processed zinc tin oxide (ZTO) thin film transistors (TFTs) were fabricated by varying the Zn/Sn composition. The addition of Sn to the zinc oxide (ZnO) films resulted in improved electrical characteristics, with devices of $Zn_{0.7}Sn_{0.3}O$ composition showing the highest mobility of 7.7 $cm^2/(V\ s)$. An improvement in subthreshold swings was also observed, indicative of a reduction of the interfacial trap densities. Mobility studies at low temperature have been carried out, which indicated that the activation energy was reduced with Sn incorporation. Kelvin probe force microscopy was performed on the films to evaluate work function and correlated to the metal−semiconductor barrier indicating $Zn_{0.7}Sn_{0.3}O$ films had the smallest barrier for charge injection. Organic−inorganic hybrid complementary inverters with a maximum gain of 10 were fabricated by integrating ZTO TFTs with poly-3-hexylthiophene (P3HT) transistors.

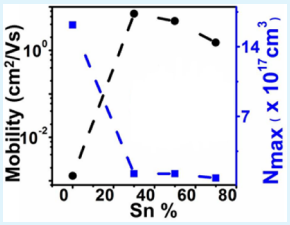

KEYWORDS: *zinc tin oxide, amorphous semiconductors, thin film transistors, CMOS inverter, Kelvin probe, solution processing*

INTRODUCTION

The recent development of thin film transistors (TFTs) using amorphous metal oxide semiconductors (AMOS) is quite promising due to advantages such as high field effect mobility, wide band gap, and simple processing techniques.[1,2] Solution based deposition techniques offer the advantage of low cost and large area coverage making them attractive for low cost electronics. High performance TFTs have been demonstrated using solution processed techniques such as spin coating,[3,4] dip coating[5] and inkjet printing.[6] Multicomponent oxides with heavy metal cations such as indium zinc oxide,[7] indium gallium zinc oxide,[8] indium zinc tin oxide,[9] and zinc tin oxide[10] (ZTO) have been used as the semiconducting channel for TFTs. In AMOS, the bottom of the conduction band is composed of metal ns orbitals, which are insensitive to bond angle distortion resulting in higher mobility in amorphous state compared to amorphous silicon[11] and organic semiconductors.[12] Due to the need for indium and gallium free semiconductors that are inexpensive and non-toxic, ZTO serves as a promising substituent semiconductor. In addition, ZTO shows chemical stability with respect to oxidation and etching[13,14] as well as physical robustness.

In these multicomponent oxides, the physical and electrical properties are largely affected by the stoichiometry of these films. In this report, we investigate the effect of Tin (Sn) concentration on the performance of solution-processed amorphous zinc tin oxide (a-ZTO) thin film transistors. The Sn concentration in the film strongly determines the carrier mobility and trap density, and its influence on the device performance is examined in detail. Low temperature charge transport studies have been carried out, and the effect of varying composition on the activation energy has been studied. In addition, we carried out Kelvin probe force microscopy (KPFM) studies on such films to evaluate the change of surface potential induced by composition change in ZTO. Optimized ZTO TFTs were combined with p-type transistors fabricated from poly-3-hexylthiophene (P3HT) to form hysteresis free complementary inverters with high gain.

EXPERIMENTAL SECTION

Synthesis of ZTO Films. The ZTO solution was prepared by mixing $ZnCl_2$ and $SnCl_2$ precursors in acetonitrile at different molar ratios; 0.136g of $ZnCl_2$ and 0.189g of $SnCl_2$ were added to 10 mL of acetonitrile solution each to make stock solution of the metal salt precursors. In order to improve the solubility of the salt precursor, 500 μL of acetic acid was added to the final precursor solution. The molar ratios of (Zn/Sn) in the final precursor solutions were varied as 1:0, 0.7:0.3, 0.5:0.5, and 0.3:0.7. The solution was stirred at 60 °C in air for 12 h and filtered using 0.2 μm filters. The stock solutions were stable and expressed no precipitation during weeks of usage.

Film Characterization. To confirm the chemical composition of the various films, X-ray photoelectron spectroscopy (XPS) measurements were carried out with a monochromatic X-ray source (Specs

Received: March 19, 2013
Accepted: December 11, 2013
Published: December 11, 2013

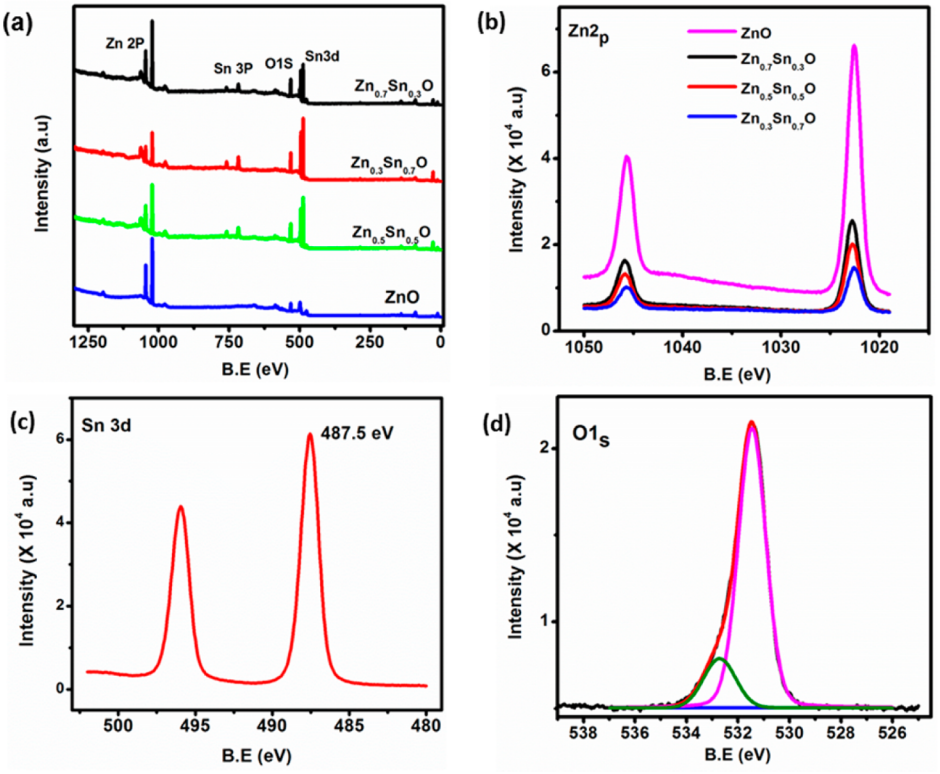

Figure 1. (a) Survey scan for ZnO and ZTO films highlighting the Zn 2p, Sn 3p, O 1s, and Sn 3d orbitals. (b) Narrow scan for Zn 2p. (c) Narrow Scan for Sn 3d. (d) Narrow scan for O 1s.

Focus 500 and Omicron EA125) at Al Kα (1486.7 eV) under ultrahigh vacuum (UHV) condition at room temperature. Surface potential measurements (KPFM) were carried out on a commercial Asylum Research MF3PD system, using a platinum-coated silicon cantilever (Olympus Model AC240 TM, resonant frequency of 70 kHz, spring constant of 2 N/m, tip height = 14 μm, and tip radius $\approx$ 30 nm). Topographic noncontact imaging was performed in frequency modulation mode, while KPFM data was recorded simultaneously in amplitude modulation mode. The surface potential was evaluated in order to extract the Fermi level of the films modified due to the composition changes introduced by the varying Sn concentration in ZTO films.

Device Fabrication. ZTO TFTs were fabricated by spin coating the solution on precleaned commercial 200 nm Si_3N_4 films on silicon (p-type, [100] oriented) substrate. The precursor solution was spin coated at 4000 rpm for 30 s resulting in a film thickness of ~15 nm measured using atomic force microscopy. The films were then annealed at 500° C for 1 h in air, and aluminum was deposited as top electrodes forming transistors of various channel lengths and channel width. Typical dimensions were 1000 μm as channel width and 100 μm as the channel length. Following the formation of the $Zn_{0.7}Sn_{0.3}O$ layer, the inverters were completed by spin coating P3HT (10 mg/mL, dichlorobenzene) on hexamethyldisilazane (HMDS) treated dielectric substrate. Gold as the source-drain electrode was thermally evaporated on both P3HT and ZTO device to give a channel length of 100 μm and channel width of 1000 μm.

Electrical Characterization. Transistor measurements were carried out in both air and vacuum using a Keithley 4200 semiconductor analyzer. No appreciable differences in the performance of the ZTO transistors were noted when measuring the devices in both conditions. Measurements of temperature dependent mobility of various Zn/Sn ratio TFT samples were conducted in the cryogenic probe station (Lakeshore-1200). To ensure performance uniformity, TFT data presented here are reported from 10 devices fabricated for each molar concentration.

RESULTS AND DISCUSSION

Physical Characteristics. The spun coated and annealed films were first analyzed using XPS to confirm the composition. Figure 1a shows the survey scans of the various prepared samples. The Zn $2p^{3/2}$ and the Sn $3d^{5/2}$ located at 1022.7 and 487.5 eV, respectively, were monitored to estimate the relative composition of the films. They were in line with the nominal compositions of the precursor solutions. Since Sn can exist in its Sn^{2+} or Sn^{4+} oxidation state (which can result in p-type SnO or n-type SnO_2), the oxidation states of samples prepared from $SnCl_2$ solutions were examined. The narrow scan for Sn 3d and O1s is shown in the Figure 1c,d. The $3d^{5/2}$ shows only one component at 487.5 eV ruling out the coexistence of SnO and SnO_2.[15,16] Since the binding energy of Sn in SnO_2 (486.3–487.1 eV) is reported to be only slightly higher than Sn in SnO (485.8–486.9 eV), the binding energy of Sn alone is not sufficient to distinguish the chemical states of the Sn sample.[17] The examination of the O1s spectrum reveals two components located at 531.5 and 532.7 eV with the higher binding energy component attributable to adsorbed hydroxyls. The atomic ratio (Sn/O) of 1:1.63 computed from Sn 3d and O1s peaks (taking into consideration atomic sensitivity factors) implies that the sample is oxygen-deficient SnO_2.[17] In addition to the composition, the morphology of the samples was also examined, ZnO displayed a granular morphology with an average rms surface roughness of ~6.8 nm, while the ZTO samples showed a smooth amorphous morphology with average surface roughness of 0.5 nm. The difference in the surface roughness may be attributed to the ZnO films being polycrystalline while the ZTO samples are amorphous (Supporting Information).[4]

dx.doi.org/10.1021/am401003k | ACS Appl. Mater. Interfaces 2014, 6, 773–777

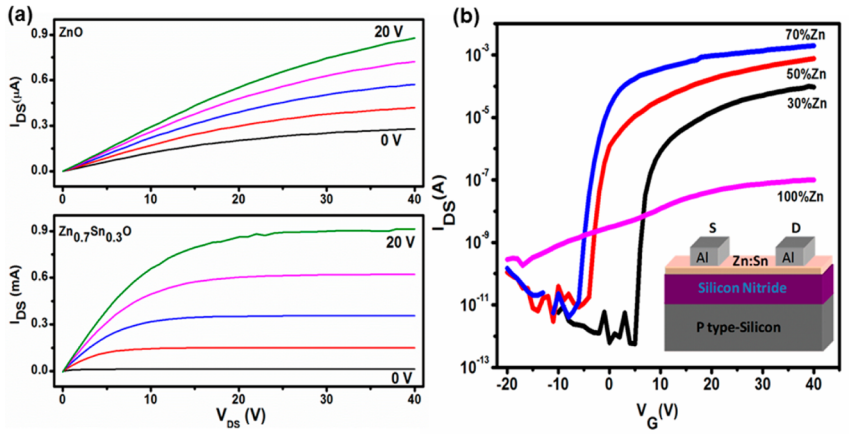

Figure 2. (a) Transistor $I-V$ characteristics for pristine ZnO and $Zn_{0.7}Sn_{0.3}O$ ratio devices with W/L 1000 μm/105 μm. (b) Transconductance response for varying Zn/Sn ratio FET fabricated on silicon nitride dielectric (inset) device architecture.

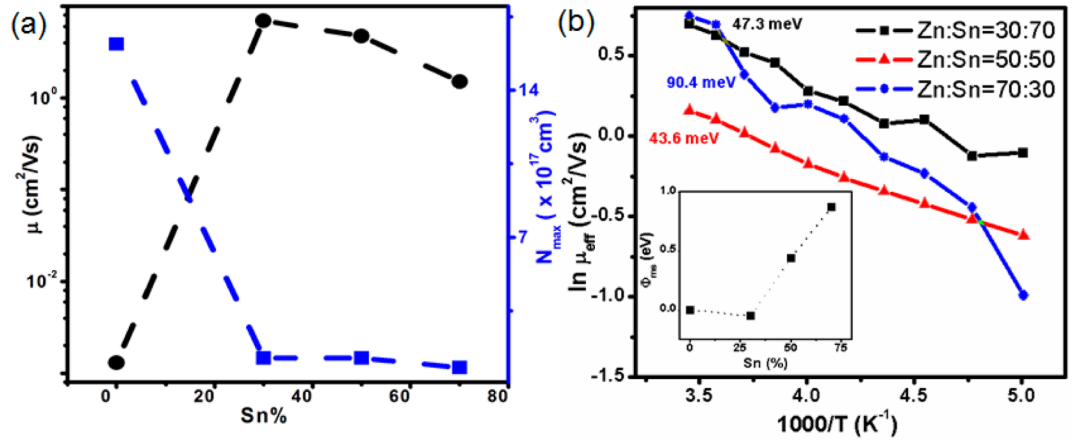

Figure 3. (a) Mobility and trap density extracted from the FET response plotted for devices with different concentrations. (b) Plot of ln μ vs $1000/T$ for Zn/Sn molar ratio samples measured at V_G of 10 V. (Inset) Work-function difference between Al electrode and the material measured using KPFM.

Electrical Characteristics. ZTO TFTs fabricated with different molar concentration with Al source drain electrodes showed n-channel transport. The saturation regime mobility (μ) and threshold voltage (V_{TH}) parameters were extracted using the standard expression,

$$I_{ds} = \frac{W\mu C_i}{L}(V_G - V_{TH})^2 \quad (1)$$

where μ is mobility, W and L is the channel length and width, C_i is gate dielectric areal capacitance, V_G is the gate voltage, and V_{TH} is the threshold voltage. Figure 2a compares the $I-V$ characteristics of pristine ZnO TFTs against $Zn_{0.7}Sn_{0.3}O$ TFTs, indicating an increase in saturation current for the same applied V_G. The addition of Sn to the ZnO films resulted in improved electrical characteristics, with devices of $Zn_{0.7}Sn_{0.3}O$ ratio showing the highest mobility of 7.7 $cm^2/(V\ s)$. The other two ratios studied yielded mobilities of 5.4 $cm^2/(V\ s)$ ($Zn_{0.5}Sn_{0.5}O$) and 1.8 $cm^2/(V\ s)$ ($Zn_{0.3}Sn_{0.7}O$), respectively. Figure 2b displays a set of representative transfer characteristics for $Zn_xSn_{1-x}O$ transistors of different Zn/Sn ratios. The mobility for all the devices was extracted from the transconductance curve at V_{ds} of 40 V. The pure ZnO TFT prepared from $ZnCl_2$ precursor shows nominal transistor characteristics with $\mu \sim 10^{-3}$ $cm^2/(V\ s)$ and on/off ratio of 10^3. The pure SnO_2 film, which did not show any gate voltage dependence, showed high conductivity indicative of high carrier density induced by oxygen vacancies. For higher Sn concentrations in $Zn_xSn_{1-x}O$, there was a slight reduction in mobility as indicated in Figure 3a. The subthreshold swing decreases with Sn content (Supporting Information), indicating that the extremely low mobility and low subthreshold slope in ZnO TFTs can be attributed to low carrier concentration and high density of surface states at the interface between the channel and gate dielectric. In particular, the grains as seen using atomic micrograph images for ZnO films may induce a significant number of interfacial states resulting in lower field effect mobility. Figure 3a shows the plot of trap density extracted for various Zn/Sn molar ratio films using the equation

$$N_{trap}^{max} = \frac{C_i}{q}\left(\frac{qs.s\log e}{k_B T} - 1\right) \quad (2)$$

where k_B is the Boltzmann constant, T is the temperature, e is the base of natural logarithm, q is the electronic charge, $s.s$ is the reciprocal of subthreshold slope, and C_i is the areal dielectric capacitance. The maximum trap density was extracted for ZnO TFT with a reduction in trap density with increasing Sn concentration in the film. On addition of Sn, the trap density reduces nearly by 2 orders of magnitude, going from 1.6×10^{18} cm^{-3} (ZnO) to 7.9×10^{16} cm^{-3} for $Zn_{0.3}Sn_{0.7}O$.

dx.doi.org/10.1021/am401003k | ACS Appl. Mater. Interfaces 2014, 6, 773−777

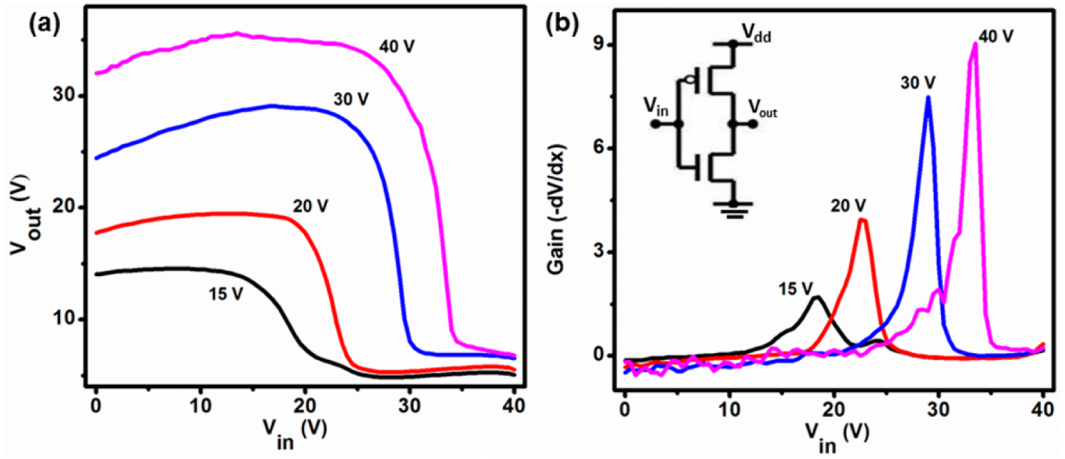

Figure 4. (a) The switching characteristics of an inverter fabricated from p-channel P3HT and n channel $Zn_{0.7}Sn_{0.3}O$ measured at various V_{dd}. (b) Corresponding gain for the inverter measured at different V_{dd}. (Inset) Shows the circuit configuration.

The effect of varying Zn/Sn concentration on charge transport was studied by extracting activation energy of these devices by measuring the performance at variable temperatures. Figure 3b shows the plot of mobility measured at saturation gate voltages measured as a function of temperature. From the plot of ln μ_{eff} vs 1000/T the activation energy E_a was estimated using the equation, $E_a = (-1000k_B)((\partial(\ln \mu)/(\partial(1000/T)))$where k_B is the Boltzmann constant and T is the temperature. All the devices showed thermally activated transport, with varying activation energy for different Zn/Sn ratio samples. Figure 3b shows the dependence of activation energy of Zn/Sn films measured at V_g of 10 V with $Zn_{0.7}Sn_{0.3}O$ films composition showing an activation energy of 90.4 meV while it reduces to ∼40−50 meV at higher Sn concentrations. This reduction in activation energy could be connected to the lower trap densities extracted previously. Although the mobility values for all the ZTO devices show performance >1 $cm^2/(V\ s)$, it is surprising that the composition which yielded the highest mobility also had the highest activation energy for electron transport. In order to investigate the possibility of injection barriers at the metal electrode−semiconductor interface affecting the performance of the devices, KPFM measurements were performed.

Surface potential of the samples were measured using KPFM by initially heating the active device at 100° C for 15 min in order to eliminate the effect of adsorbed moisture on the samples. The samples showed a distinct variation of surface potential as a function of Sn composition in ZnO films. The incorporation of Sn atoms to ZnO matrix resulted in an increase of the surface potential. The KPFM measurements have been used to evaluate the surface potential of ZTO films, which is indicative of work function of the sample, based on the equation $\Delta SP = (\varphi_{tip} - \varphi_s)/e$, where φ_{tip} is the work function of the tip (Pt coated on Si) and φ_s is that of the sample. The aluminum electrode (ϕ_m = 4.2 eV) used as the source-drain electrode of the ZTO FETs is used as an internal reference directly on each sample. The difference in the work function of Al and ZTO film has been used to calculate the injection barrier for each of the samples.[18−20] The work-function difference (ϕ_{ms}) between the Al electrodes and the KPFM measured work-function of ZTO is plotted in the inset of Figure 3b. The addition of Sn resulted in an increased barrier for electron injection with $Zn_{0.7}Sn_{0.3}O$ films showing the lowest barrier. This low injection barrier coupled with lower trap density (due to Sn addition) could be the reason why ZTO films of (0.7:0.3) composition have the best performance. These general trends still hold true for samples fabricated at finer concentration intervals with samples lower than 30% Sn concentrations not resulting in high mobility devices (Figure S3, Supporting Information). Although the fabrication procedures utilized for fabricating these amorphous thin films requires a rather high annealing temperature of 500 °C (incompatible with plastic substrates), the trends in the mobility values, as well as trap densities extracted here, should be applicable to films formed through low temperature recipes such as combustion synthesis.[21]

On the basis of the optimized performance for $Zn_{0.7}Sn_{0.3}O$ TFT, complementary inverters were fabricated using P3HT-ZTO TFTs. The schematic representation of the electrical connections is shown in the inset of Figure 4b. In the circuit, the input voltage V_{in} was applied to the common gate for both transistors. Plots of the output voltage V_{out} as a function of V_{in} under the different supply voltages V_{dd} are shown in Figure 4a. No hysteresis was observed during the inverter action, reflecting excellent threshold voltage stability in devices. The measured voltage gain $-dV_{out}/dV_{in}$, an important parameter for subsequent stage switching, was of the order of ∼10 and 3 at V_{dd} of 40 V and V_{dd} of 15 V. As expected, the gain and switching point increases with applied V_{dd}.[22] From the inverter output characteristics at V_{dd} = 40 V, an input high voltage (V_{IH}) of 8.5 V and input low voltage (V_{IL}) of 9.8 V could be measured at unity gain. Similarly, the devices have high and low output voltages of 12.7 and 7.8 V, which gives a low noise margin (M_{LN}) of 1.8 V and high noise margin (M_{HN}) of 4.2 V.

CONCLUSION

In summary, the effect on Zn/Sn composition change on the electrical characteristics was studied by fabricating solution processed ZTO FETs. The Zn/Sn composition ratio clearly has an effect on film morphology, electrical property, and surface potential. The addition of Sn concentration causes a significant improvement of FET performance with a maximum mobility of 7.7 $cm^2/(V\ s)$. The increased Sn concentration is accompanied by a reduction in the trap densities within these devices as well as a modulation of the injection barrier at the metal−semiconductor junction. Reduced trap densities as well as low injection barrier between the electrode and ZTO films

determine the composition with the highest performance. Complementary inverters were fabricated, utilizing the optimized n-type ZTO composition along with p-type P3HT films. This work demonstrates the potential of optimized ZTO FETs fabricated through a solution processed approach.

■ ASSOCIATED CONTENT

Supporting Information

Subthreshold swing values as well as atomic force microscopy measurements on the thin films. This information is available free of charge via the Internet at http://pubs.acs.org/

■ AUTHOR INFORMATION

Corresponding Author

*E-mail: Nripan@ntu.edu.sg.

Author Contributions

#R.D.C. and M.R. contributed equally.

Notes

The authors declare no competing financial interest.

■ ACKNOWLEDGMENTS

The project was supported by A*STAR, Project No: 102 170 0318, and NRF-CREATE funding under the SinBeRISE program.

■ REFERENCES

(1) Nomura, K.; Ohta, H.; Takagi, A.; Kamiya, T.; Hirano, M.; Hosono, H. *Nature* **2004**, *432*, 488−492.
(2) Park, J. S.; Maeng, W. J.; Kim, H.S.; Park, J. S. *Thin Solid Films* **2012**, *520*, 1679−1693.
(3) Banger, K. K.; Yamashita, Y.; Mori, K.; Peterson, R. L.; Leedham, T.; Richard, J.; Sirringhaus, H. *Nat. Mater.* **2011**, *10*, 45−50.
(4) Oo, T. Z.; Devi Chandra, R.; Yantara, N.; Prabhakar, R. R.; Wong, L. H.; Mathews, N.; Mhaisalkar, S. G. *Org. Electron.* **2012**, *13*, 870−874.
(5) Pal, B. N.; Dhar, B. M.; See, K. C.; Katz, H. E. *Nat. Mater.* **2009**, *8*, 898−903.
(6) Lee, D. H.; Han, S. Y.; Herman, G. S.; Chang, C.H. *J. Mater. Chem.* **2009**, *19*, 3135−3137.
(7) Park, K. B.; Seon, J. B.; Kim, G. H.; Yang, M.; Koo, B.; Kim, H. J.; Ryu, M. W.; Lee, S.Y. *IEEE Electron Device Lett.* **2010**, *31*, 311−313.
(8) Kim, H. G.; Ahn, B. D.; Shin, H. S.; Jeong, W.H.; Kim, H.J. *Appl. Phys. Lett.* **2009**, *94*, 233501−233503.
(9) Ryu, M. K.; Yang, S.; Park, S. H.; Hwang, C.-S.; Jeong, J.K. *Appl. Phys. Lett.* **2009**, *95*, 173508−173510.
(10) Lee, C. G.; Dodabalapur, A. *Appl. Phys. Lett.* **2010**, *96*, 243501−243503.
(11) Nomura, K.; Ohta, H.; Takagi, A.; Kamiya, T.; Hirano, M.; Hosono, H. *Nature* **2004**, *432*, 488−492.
(12) Nomura, K.; Ohta, H.; Ueda, K.; Kamiya, T.; Hirano, M.; Hosono, H. *Science* **2003**, *300*, 1269−1272.
(13) Minami, T.; Takata, S.; Sato, H.; Sonohara, H. *J. Vac. Sci. Technol.* **1995**, *A13*, 1095−1099.
(14) Young, D. L.; Moutinho, H.; Yan, Y.; Coutts, T. J. *J. Appl. Phys.* **2002**, *92*, 310−319.
(15) Hwang, S.; Kim, Y. Y.; Lee, J. H.; Seo, D. K.; Lee, J. Y.; Cho, H. K. *J. Am. Ceram. Soc.* **2012**, *95*, 324−327.
(16) Kövér, L.; Kovács, Zs.; Sanjinés, R.; Moretti, G.; Cserny, I.; Margaritondo, G.; Pálinkás, J.; Adachi, H. *Surf. Interface Anal.* **1995**, *23*, 461−466.
(17) Choi, W. K.; Sung, H.; Kim, K. H.; Cho, J. S.; Choi, S. C.; Jung, H.-J.; Koh, S. K.; Lee, C. M.; Jeong, K. *J. Mater. Sci. Lett.* **1997**, *16*, 1551−1554.
(18) Bürgi, L.; Richards, T. J.; Friend, R. H.; Sirringhaus, H. *J. Appl. Phys.* **2003**, *94*, 6129−6137.
(19) Khaderbad, M. A.; Tjoa, V.; Rao, M.; Phandripande, R.; Madhu, S.; Wei, J.; Ravikanth, M.; Mathews, N.; Mhaisalkar, S. G.; Rao, V. R. *ACS Appl. Mater. Interfaces* **2012**, *4*, 1434−1439.
(20) Liscio, A.; Veronese, G.P.; Treossi, E.; Suriano, F.; Rossella, F.; Bellani, V.; Rizzoli, R.; Samori, P.; Palermo, V. *J. Mater. Chem.* **2011**, *21*, 2921−2931.
(21) Kim, M. G.; Kanatzidis, M. G.; Facchetti, A.; Marks, T. J. *Nat. Mat.* **2011**, *10*, 382−388.
(22) Tan, H. S.; Wang, B. C.; Kamath, S.; Chua, J.; Shojaei-Baghini, M.; Rao, V. R.; Mathews, N.; Mhaisalkar, S. G. *IEEE Electron Device Lett.* **2010**, *31*, 1311−1313.